# Energy transfer processes in ZnSe/(Zn,Mn)Se double quantum wells

Stephanie Jankowski, Swantje Horst, Alexej Chernikov, Sangam Chatterjee, and Wolfram Heimbrodt
*Faculty of Physics and Material Sciences Center, Philipps-Universität Marburg, Renthof 5, D-35032 Marburg, Germany*
(Received 7 July 2009; published 12 October 2009)

The complex interplay of energy transfer and tunneling processes in a series of asymmetric ZnSe/(Zn,Mn)Se double quantum-well (DQW) structures is investigated. Steady-state and time-resolved photoluminescence at low temperatures and external magnetic fields up to 7 T in this system show remarkable differences to earlier studies on CdTe/(Cd,Mn)Te DQWs. The pure quantum-mechanical tunneling process is only a minor contribution to the magnetic field dependence of the emission even in case of small barriers and strong QW coupling. The experimental results are supported by quantum-well calculations.

DOI: 10.1103/PhysRevB.80.155315 PACS number(s): 75.50.Pp, 78.55.Et, 78.67.De, 71.70.Gm

## I. INTRODUCTION

Asymmetric double quantum-well (DQW) structures with magnetic barriers and nonmagnetic wells were frequently used to investigate the fundamental quantum-mechanical tunneling processes in the past.[1–12] The unequal well widths lead to different energy states in the QWs. Particularly, the role of exciton versus independent electron-hole tunneling as well as the influence of phonons was studied in wide-gap semiconductor heterostructures.

Tunneling of spatially direct excitons is very efficient when mediated by phonon emission or via resonance with 2*s* states of the lower-energy QW.[12] Later it was shown that the tunneling of excitons as a whole entity with the emission of only one-LO phonon is very slow. The tunneling via spatially indirect states in a two-step process, however, is strongly enhanced by electron-hole interaction.[1] Generally, an efficient exciton transfer is possible for effective two-LO phonon scattering as well as even below a one-LO phonon energy. The latter effect is explained by a radiationless resonance energy transfer since acoustic-phonon scattering yields orders of magnitudes smaller tunneling probabilities.[4]

DQW structures with a semimagnetic inner barrier are ideal systems for studying such questions. The "giant" Zeeman splitting, associated with the *s*-*d* and *p*-*d* exchange interaction between the extended band states and the localized Mn 3*d* states, allows for the effective tuning of the inner barrier. The exponential dependence of the tunneling probability on the barrier height yields a huge variation in the tunneling process in external magnetic fields and thus allows for a detailed investigation of the tunneling. Typical measurements were performed, e.g., on CdTe/(Cd,Mn)Te DQW structures.[12–18] The luminescence intensity of the wide well (WW) increases when reducing the inner barrier whereas the higher-energy luminescence of the narrow well (NW) decreases. The results were in perfect concordance with time-resolved measurements. The supposedly similar ZnSe/(Zn,Mn)Se material system, where also just the semimagnetic barriers varies in an external magnetic field, should thus not yield any additional information; the larger band gaps of ZnSe and (Zn,Mn)Se shift the corresponding exciton energies further into the blue spectral range while the fundamental physics should be the same. However, tremendous differences are found when comparing the optical properties of ZnSe/(Zn,Mn)Se DQWs with earlier measurements on CdTe/(Cd,Mn)Te DQWs. Taking a closer look, however significant differences between the two material systems are revealed in the following two aspects: first, the ZnSe QWs are under tensile strain yielding the light-hole (lh) valence-band states as the lowest-lying states in energy. Traditionally, systems with heavy-hole (hh) excitons as lowest-lying state are investigated. Second, the band gaps of both ZnSe wells and (Zn,Mn)Se barriers are larger than the internal 3*d* transition of the $Mn^{2+}$ ions. In this paper it is shown that the pure tunneling behavior is camouflaged. The magnetic field dependence of the luminescence is a result of the complicated interplay between various energy transfer processes and tunneling in this type of structures.

## II. SAMPLES AND EXPERIMENTAL METHODS

A series of three asymmetric DQW structures grown on a 750-nm-thick ZnSe buffer on (100)-oriented GaAs substrate are investigated. In the following, the samples are labeled dqw100, dqw10, and dqw5 according to the width of their inner barrier of 100, 10, and 5 nm, respectively. The narrow well has a width of about 2.3 nm and the wide well of about 5.7 nm in all samples. The wells are embedded between (Zn,Mn)Se cladding layers with a Mn concentration of 28% in case of dqw10, 30% for dqw5, and 34% in case of dqw100 as asserted by x-ray diffraction and reflection high-energy electron-diffraction measurements. This design yield tensile-strained ZnSe QWs between (Zn,Mn)Se barriers because of the different lattice constants of ZnSe ($a_{ZnSe}$=5.669 Å) and (Zn,Mn)Se ($a_{Zn_{0.66}Mn_{0.34}Se}$=5.72 Å).

The samples are investigated by both continuous-wave (CW) and time-resolved (TR) photoluminescence (PL). For the CW measurements, the samples are immersed in liquid helium at a temperature of 1.9 K inside the cryostat of a superconducting magnet system. Magnetic fields up to $B$ =7 T are generated at the position of the sample. An argon-ion laser at 3.53 eV (λ=351.1 nm) is used for excitation. The photoluminescence is imaged onto a spectrometer equipped with a charge-coupled device detector used for recording the spectra. The TRPL experiments are carried out at a lattice temperature of 10–15 K inside a contact-gas cryostat in a different superconducting magnetic system capable of fields up to 14 T. A mode-locked Ti:sapphire laser is used for

 ©2009 The American Physical Society

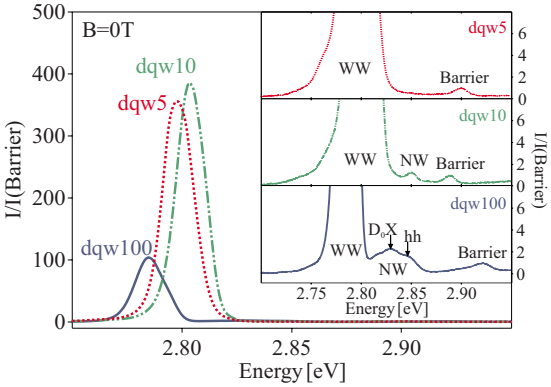


FIG. 1. (Color online) PL of the samples dqw100 (solid blue line), dqw10 (dashed dotted green line), and dqw5 (dotted red line) without an external magnetic field. The PL is normalized to the maximum of the barrier emission intensity. The strongest luminescence comes from the WW for all samples. The emission from the NW and barriers is shown in the respective insets.

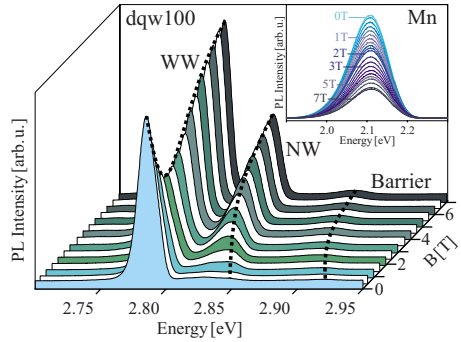


FIG. 2. (Color online) CW PL emission from sample dqw100. The external magnetic field is scanned from 0 to 7 T in steps of 0.1 T up to 4 T, followed by steps of 0.2 T up to 5 T, as well as 5.25, 5.5, 6, 6.5, and 7 T. The dashed line shows the maxima of the PL as a guide to the eyes. The inset shows the emission from the manganese in this structure.

excitation and a streak-camera system for detection yielding a time resolution of down to 800 fs.

## III. EXPERIMENTAL RESULTS AND DISCUSSION

First, the steady-state behavior at zero magnetic field is discussed. Figure 1 shows the corresponding PL spectra of all three heterostructures. The PL spectra from all three samples are normalized to the respective maximal intensity of the barriers. The strong low-energy peaks for dqw100 at 2.785 eV, for dqw10 at 2.804 eV, and at 2.798 eV for dqw5 are assigned to the WW. The differences in energy are caused by the slightly varying well widths. The inset of Fig. 1 shows the emission on a magnified scale revealing clearly the weak emission from the NW and the barrier. Two additional bands are observed from the NW for sample dqw100 at 2.83 and 2.845 eV. These are identified as the $D^0X$ and the hh exciton as will be discussed below. The sample dqw10 shows the NW signal at 2.851 eV while no specific steady-state NW signal is identified for the sample with the thinnest inner barrier of only 5 nm in the CW spectra. The (Zn,Mn)Se barrier emission is found at 2.921 eV for the dqw100, at 2.889 eV for dqw10, and at 2.901 eV for the dqw5, which corresponds to the slightly different Mn concentrations in the samples. The barrier PL as well as the NW PL are considerably weaker than the WW PL due to relaxation and tunneling processes. Furthermore, it is anticipated that the NW PL is weaker for a thinner inner barrier due to the enhanced NW-WW tunneling as can clearly be seen in Fig. 1.

While these results may not appear extraordinary at a first glance it should be noted that tunneling through a 100-nm-thick barrier is rather unlikely. Thus, it is surprising that the NW PL is already very weak even in the case of dqw100. This is explained by the following two reasons: on the one hand, it is of course possible to overcome even an inner barrier of 100 nm by dipole-dipole interaction. On the other hand, the Mn subsystem in the barriers acts as additional drain for the excitation of both QWs by a Förster-type radiationless energy transfer (FRET).[19] This channel is, however, more efficient for the NW states compared to the WW states due to the stronger penetration of exciton wave functions into the barriers caused by the stronger confinement. This transfer is efficient since the QW PL is resonant to the broad $^6A_1 \rightarrow {}^4E_1$, $^4A_1$ $3d$ internal transition. The WW PL is smallest in the dqw100. This becomes clear for three reasons, (i) no tunneling is expected and (ii) the Mn concentration in the barrier is higher as can be seen in Fig. 1. The FRET rate is proportional to the Mn concentration (see, e.g., Ref. 20) and the FRET transfer is therefore somewhat stronger in the dqw100 compared to the other samples. (iii) The higher Mn concentration introduces additional lattice imperfections and respective radiationless centers at the interface and in the barriers

Next, the influence of the magnetic field on the CW PL is investigated. The PL of dqw100 is depicted in Fig. 2 for varying magnetic field strengths up to 7 T. Clearly, the WW PL decreases up to a critical-field strength of about 2.4 T and then increases again with increasing magnetic field strengths. At the same time, the emission from the NW continuously increases while the manganese PL (inset of Fig. 2) is decreasing with rising magnetic fields. This behavior is very much the same for the dqw10 and dqw5. Concerning the expected tunneling the intensity dependence on the magnetic field strength is rather strange. For example, the magnetic field dependence is completely different for the CdTe/(Cd,Mn)Te DQW systems.[17] There, the reduction in the barrier height in an external magnetic field due to the giant Zeeman effect leads to increasing emission from the WW accompanied by a decreasing emission from the NW, i.e., the tunneling probability from the NW to the WW is enhanced as anticipated. This seemingly totally different behavior between the ZnSe/(Zn,Mn)Se and CdTe/(Cd,Mn)Te DQWs is explained as follows: the lowest exciton state in the ZnSe-WW is the lh exciton caused by the tensile strain in the wells. The Zeeman splitting and the sequence of the lh and hh states in the strained system have been studied in an earlier paper.[21] The conduction band splits into the lower and higher energy $|\frac{1}{2},-\frac{1}{2}\rangle$ and $|\frac{1}{2},\frac{1}{2}\rangle$ ($el_-$ and $el_+$) states in an external magnetic field as a result of the giant Zeeman effect of the barriers as illustrated on the left side of Fig. 3. The

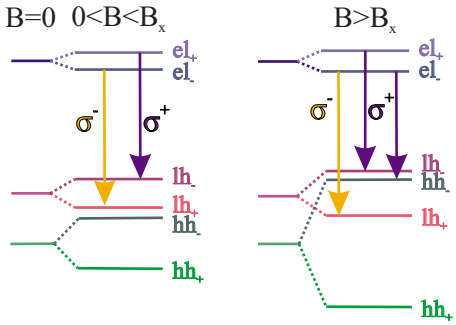


FIG. 3. (Color online) Level scheme of the Zeeman splitting for the WW in the case of different magnetic fields and their dipole allowed transitions in Faraday configurations. The left side shows the splitting for the electrons and holes for low magnetic fields ($B < B_x$), where the lh_ are the lowest in energy. The probability for the $\sigma^+$ transition decreases as the magnetic field increases due to the lower el$_+$ occupation. At the same time the $\sigma^-$-transition probability decreases as the lower lh$_+$ occupation. The $\sigma^+$ transitions are stronger than the $\sigma^-$ transition since the conduction-band splitting is smaller than the valence-band splitting in external magnetic fields. On the right side, the splitting for higher magnetic fields ($B > B_x$) is shown. The hh states has a three times stronger splitting than the lh leading to a crossover of the hh and lh states. The $\sigma^+$ transition between the lowest electron state and the lowest hh (el_-hh_) become dominant for $B > B_x$ and its transition probability increases with increasing magnetic field.

conduction-band splitting of the (Zn,Mn)Se barriers is described by (see, e.g., Refs. 22 and 23)

$$\Delta E^{cb} = a x_{\mathrm{Mn}} N_0 \alpha S B_S(\xi) m_j, \quad m_j = \pm \frac{1}{2}. \tag{1}$$

Here, the Mn concentration is $x_{\mathrm{Mn}}$, $N_0$ denotes the number of unit cells per cm$^{-3}$, $\alpha$ is the $s$-$d$ exchange-interaction parameter, and $m_j$ is the magnetic quantum number. $S$ is the spin of the Mn ions and $B_S(\xi)$ is the associated Brillouin function. The factor $a$ is a value between 0 and 1 modifying the Brillouin function[24] and describing the reduction in the effective Mn concentration by clustering of Mn ions and consequential antiferromagnetic coupling. The corresponding splitting of the valence-band states are given by

$$\Delta E^{vb} = \frac{1}{3} a x_{\mathrm{Mn}} N_0 \beta S B_S(\xi) m_j, \quad m_j = \pm \frac{1}{2}, \pm \frac{3}{2}. \tag{2}$$

The exchange integral is now $N_0\beta$, where $\beta$ is the $p$-$d$ exchange-interaction parameter. The splitting of the barrier potentials [Eqs. (1) and (2)] results in the respective field-dependent splitting of the exciton states in the QW.

The QW-lh splits into the $|\frac{3}{2},-\frac{1}{2}\rangle$ and $|\frac{3}{2},\frac{1}{2}\rangle$ states (lh_ and lh$_+$), respectively. However, the lowest-energy transition between el_ and lh_ is dipole forbidden in Faraday configuration. The occupation of the electron state el$_+$ decreases with increasing magnetic field. Hence, the allowed $\sigma^+$ transition between el$_+$ and lh_ becomes weaker with increasing external magnetic field. The same is true for the $\sigma^-$ transition between el_ and lh$_+$ because of the decreasing occupation of holes in the lh$_+$ state. Thus in conclusion, the WW signal in Fig. 2 decreases. Note that the exchange interaction is stronger for the valence band than for the conduction band. Hence, the splitting for the valance-band states is higher and the $\sigma^-$ signal decreases faster than the $\sigma^+$ signal.

Another important fact is that the splitting is stronger for the hh than for the lh because of the higher magnetic quantum number. If the magnetic field is high enough, i.e., above a critical-field strength $B_x$, the exciton state of the hh (el_-hh_), which has a $\sigma^+$ transition crosses the lh excitons (el_-lh$_+$ and el$_+$-lh_). This situation is illustrated on the right side of Fig. 3. The occupation of the hh states increase continuously as the magnetic field increases. Thus, the transition probability becomes stronger and the WW-PL increases above the critical-field strength $B_x$. This explains the rising intensity seen in Fig. 2 beyond 2.5 T.

The QW states have been modeled in the framework of an one-dimensional Schrödinger equation incorporating the strain effect, the exciton binding energies, and the influence of the giant Zeeman splitting. The investigated DQW structures are strained to a lattice constant $a_L = \alpha a_{\mathrm{ZnSe}} + (1-\alpha) a_{(\mathrm{Zn,Mn})\mathrm{Se}}$. The lattice strain factor $\alpha$ accounts for the fact that the ZnSe QW are not 100% tensile strained. Thereby, the conduction-band offset (CBO) to valence-band offset (VBO) ratio in the strain-free case is set to 0.65/0.35 for the samples with $x_{\mathrm{Mn}} \approx 0.3$. This value is fixed by the type I-type II transition as will be shown in the following. The value is somewhat higher than the value determined earlier for a ZnSe/ZnMnSe system with $x_{\mathrm{Mn}} \approx 0.25$ (Ref. 21) and higher than the value reported for a system with $x_{\mathrm{Mn}} \approx 0.20$.[25] The increasing CBO-VBO ratio with increasing manganese concentration was reported earlier for the ZnSe/ZnMnSe heterosystem on the basis of a detailed analysis of well width and concentration dependence.[26]

The resulting exciton energies for the NW and WW are depicted in the Figs. 4(b) and 4(c), respectively, with the hh excitons in green solid lines and the lh excitons are in red. The black dotted line represents the energy of the PL maxima taken from the CW measurements. The little remaining differences between the theoretical curves and experimental results are caused by the disorder-induced stokes shift, which is typically about 10 meV for the barrier and QW excitons. The stokes shift is slightly reduced with increasing field in case of the WW states as can be seen in Fig. 4(c). This is due to the lh-hh crossover and the fact that the lh excitons are more sensitive to strain fluctuations than the hh excitons.[27] The respective small valence-band offset results in a type I-type II transition in a significantly strong external magnetic field. The type transition has been observed for various Mn concentrations of the ZnSe/(Zn,Mn)Se heterosystem and the influence on the spatially indirect excitons was discussed earlier.[25,27–29] The dashed lines in Fig. 4 represents the type II excitons consisting of electrons localized in the QW and hh localized in the barriers. This point will be addressed below.

Now, the magnetic field behavior of the NW is considered. The magnetic field dependence is different for the NW than for the WW. The hh exciton in the NW is the lowest-energy state even without external field [see also Fig. 4(b)] due to the stronger confinement effect. Thus, no crossing between hh and lh excitons with increasing field can be ob-

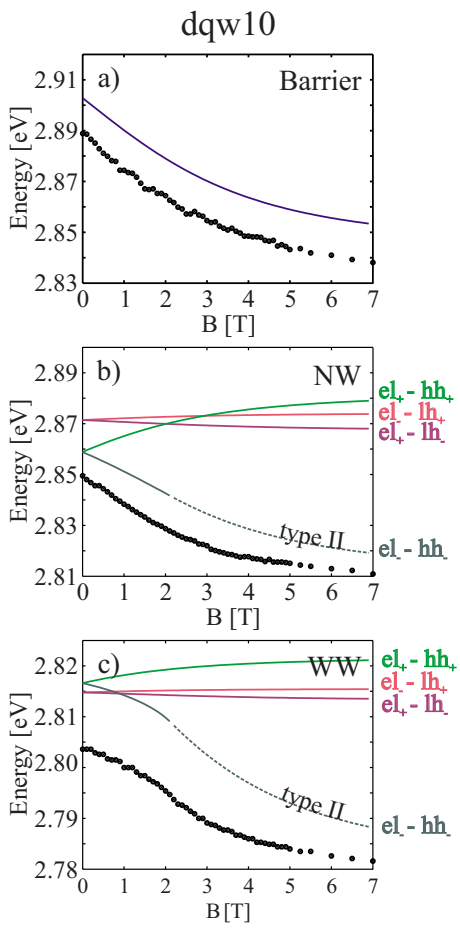


FIG. 4. (Color online) Calculated exciton energies (solid lines) as a function of the applied magnetic field using a CBO of 0.75 and a $\alpha$ of 0.45. (a) shows the lowest barrier exciton energy and there corresponding barrier emission (dots) of sample dqw10, (b) and (c) displays the calculated exciton position (lines) and the PL data (dots) for the NW and the WW.

served in the PL spectra as only the lowest state in energy is involved.

The large band gap of ZnSe and (Zn,Mn)Se enables energy transfer process from the exciton states to the internal $3d$ transitions of the Mn subsystem in the barrier. This is the most striking difference between the CdTe/(Cd,Mn)Te and the ZnSe/(Zn,Mn)Se QW structures. This radiationless FRET dominates the magnetic field dependence of the NW PL. The internal Mn PL decreases with increasing field strength whereas the NW PL increases as can be seen from the inset of Fig. 2 due to the reduced dipole-dipole transfer with increasing magnetic field.

The spin conservation plays a major role in the energy transfer process. The excitation within the $Mn^{2+}$ $3d^5$ shell (i.e., the excitation of an electron from the $^6A_1$ ground state to the $^4T_1$ first-excited state) is a dipole-forbidden transition and requires $\Delta S|_{exc}=+1$. The overall spin conservation rule can thus be fulfilled by an energy transfer from dark exciton states or bound exciton states. The dominant mechanism in ZnSe-based diluted magnetic semiconductors used to be the energy transfer via donor-bound excitons $D^0X$ as depicted in Fig. 5 (see, e.g., Ref. 30). A bright exciton alone such as the

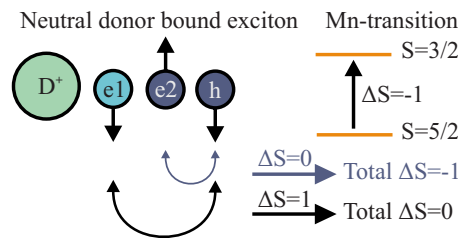


FIG. 5. (Color online) Energy transfer mechanisms from the exciton state in the QW into the internal Mn transition. It is mediated by the neutral donor-bound exciton $D^0X$ for which the total spin is conserved.

$e2+h$, can only contribute a subprocess $\Delta S|_{exc}=0$ when transferring by recombination its energy into the Mn subsystem. Hence, the total spin conservation is violated. The situation changes in the case of a donor-bound exciton. The hole $h$ can recombine with the $e1$ within the $D^0X$ complex instead of $e2$, yielding a spin contribution of $\Delta S|_{exc}=+1$ and thus allowing the conservation of the total spin $\Delta S|_{tot}=0$.

The $D^0X$ complex becomes destabilized when an external magnetic field is applied. The formation of a $D^0X$ complex requires the spin of the exciton electron $e2$ ($\uparrow$) and that of the electron bound to the neutral donor $e1$ ($\downarrow$) to be antiparallel as both electrons occupy the same state in real space. The effective binding energy between the free exciton and the $D^0X$ state decreases with increasing magnetic field. Eventually, the free exciton intersects the $D^0X$ energy yielding the lower-lying state as shown schematically in the inset of Fig. 6. This dwindling energy transfer channel to the Mn subsystem is responsible for the decreasing Mn PL as shown for dqw100 in the inset of Fig. 2. The rising PL intensity of the NW and barriers are also a consequence of this decreasing energy transfer to the Mn subsystem with increasing magnetic field. Figure 6 shows the intensity of the NW PL emission normalized to the respective intensity maximum for magnetic fields up to 2.5 T in steps of 0.5 T. The signal of both the $D^0X$ and the free hh exciton is observed for low magnetic fields. When increasing the magnetic fields from 0 to 2 T, the hh exciton shifts to lower energies and becomes stronger relative to that of the $D^0X$ until the $D^0X$ emission has almost disappeared.

Figures 7 and 8 display the normalized intensities of the PL maxima of all three samples as a function of the external magnetic field for comparison. All samples show a very similar behavior for the WW emission but the value of the critical-field strength $B_x$, indicated by arrows, is different. This is caused by slightly different Mn concentrations and the respective complex interplay of barrier height, strain, and effective exchange integral on the QW states.

The sample dqw10 containing the lowest manganese concentration shows another distinct kink in its magnet field dependent PL intensity at about 3 T. The decrease in the PL intensity is caused by the type I$\rightarrow$type II transition. The electrons are still localized in the ZnSe layers. However, the higher the external field the more the holes get localized in the (Zn,Mn)Se layers and the respective transition probabilities of the spatially indirect excitons are reduced. The type transition is confirmed by the QW calculations shown as

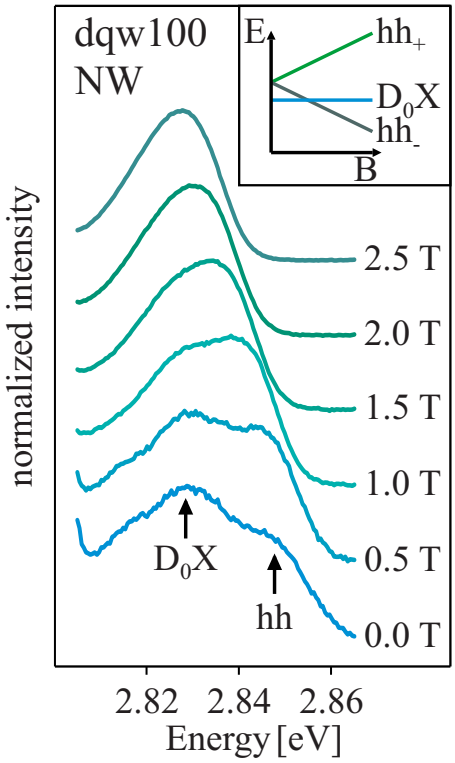


FIG. 6. (Color online) dqw100 PL of the NW normalized to its maximum. The hh exciton becomes the important one for higher magnetic fields. The inset shows the energy of the $D_0X$ exciton and the hh exciton in dependency of the magnetic field. The hh_ becomes the favored in energy for higher fields.

dashed green line in Fig. 4(c). As a consequence of this type transition the PL intensity decreases as radiationless transitions become more likely.

The barrier height are the same for the NW and the WW hence the type transition exist also for the NW at nearly the same magnetic field. The transition is observable in the intensity behavior shown in Fig. 8; it leads to a decreasing of the NW PL, too. This behavior is also in concordance with the calculations as can be seen in Fig. 4(b). The interesting

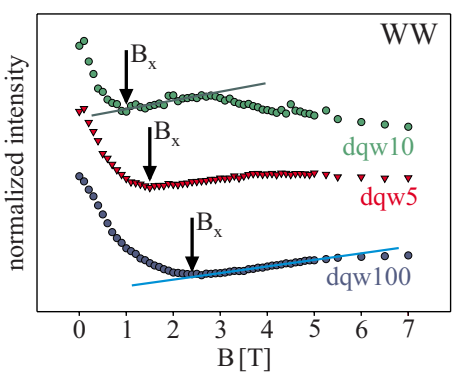


FIG. 7. (Color online) The intensity maxima of the WW emission for all three samples as a function of external magnetic field. The resulting curves are normalized to one and shifted in intensity. The point of the lowest WW maximum $B_x$ is marked for each sample.

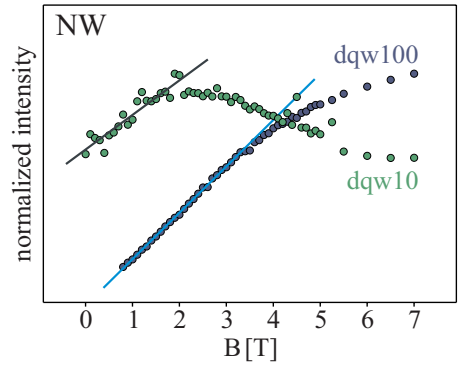


FIG. 8. (Color online) The intensity maxima of the NW emission for the samples dqw100 and dqw10 as a function of external magnetic field. The resulting curves are normalized to one.

exciton el_-hh_ [el_ of the ZnSe quantum well and hh_ of the (Zn,Mn)Se barrier] are shown just as dark green dotted line.

The kink, which is caused by the type transition, is found at about 4 T in case of sample dqw5 in concordance with the model calculations. No NW cw-signal was detectable in that sample. The type transition for the sample dqw100 is expected beyond 5 T according to the QW calculations. Therefore the respective kink in the PL intensity of the WW is hardly observable in Fig. 7. The different magnetic fields for the type transitions are also caused by the varying Mn concentrations of the samples. The NW signal in that sample increases all the way up to 7 T (see Fig. 8) because of the overwhelming effect of decreasing energy transfer into the Mn subsystem. The intensity of the barrier signal increases also with increasing magnetic field for all three samples (not shown here) for the same reason.

Next, any indication for a tunneling process and a respective change in the tunneling probability in an external magnetic field are investigated. The smaller the inner barrier, the smaller the steady-state NW PL as shown in the inset of Fig. 1. This is explained only by the enhanced tunneling probability in zero field. In an external magnetic field the inner barrier is reduced due to the giant Zeeman effect of (Zn,Mn)Se and a further enhanced tunneling is anticipated. Obviously, only a small field range can be used to look for this field effect. Actually, it is the range between $B_x$ the lh-hh crossover and the type transition. Unfortunately even there, the tunneling is covered by the energy transfer from NW and WW excitons to the internal Mn $3d$ states. Therefore, the ratio of the slopes of the WW and NW are compared in this range (indicated as solid lines in Figs. 7 and 8). The dipole-dipole transfer is not field dependent. The ratio of the slopes is given by

$$\frac{m_{\text{dqw100 WW}}}{m_{\text{dqw100 NW}}} \approx 1.3 \pm 0.5. \tag{3}$$

Notably, the intensity ratio is approximately 1 within the error bars, which indicates that the tunneling probability for the dqw100 can be assumed to be negligible as expected. The slightly stronger increasing WW intensity as can be seen in Fig. 2 can be explained as follows. As shown in Fig. 2 as well, even the barrier PL increases as the number of free

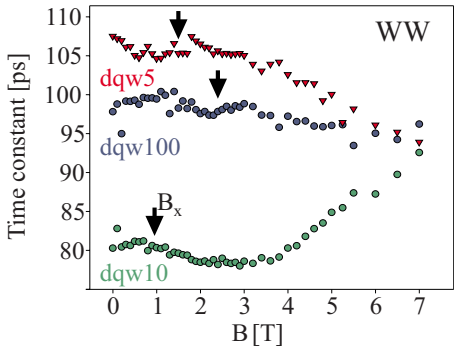


FIG. 9. (Color online) The decay time of the WW signal in dependency of the external magnetic field.

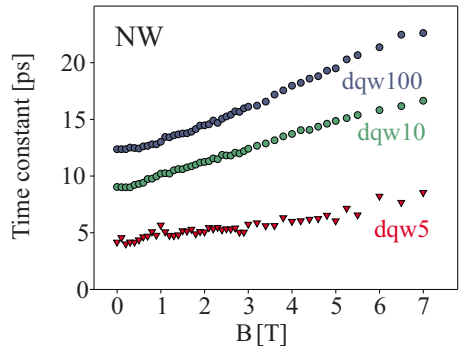


FIG. 10. (Color online) The decay time of the NW signal in dependency of the external magnetic field. The NW luminescence is only observable on the ultrafast time scale.

excitons increases due to the reduced capturing by Mn ions. The deviation from unity of the WW-NW slope ratio is a result of the higher capture cross section of the WW. The slope ratio for the dqw10 is given by

$$\frac{m_{\text{dqw10 WW}}}{m_{\text{dqw10 NW}}} \approx 100 \pm 20. \tag{4}$$

The ratio is considerably larger for dqw10. Thus, the tunneling from NW to WW becomes more likely in an external magnetic field besides the reduced transfer to Mn ions and the enhanced capture rate of barrier excitons. A similar discussion is not possible for the sample with the thinnest inner barrier, dqw5, as no NW signal was observable in the CW emission spectrum at all field strengths due to the strong NW-WW coupling and the respective high tunneling rate. If the inner barrier is thin enough tunneling is also observable in the present structures. But the other effects such as the lh-hh crossover of the WWs, the transition from type I to type II for the WW and NW, and the energy transfer to the Mn subsystems have more influence on the PL of the samples.

In addition, the samples are investigated using time-resolved photoluminescence to support these findings. In all cases, the samples are excited well above the (Zn,Mn)Se gap energy: 2.938 eV for sample dqw100, 3.179 eV for dqw10, and 3.100 eV for dqw5, preferentially creating carriers in the barrier layers. The external magnetic field was scanned from 0 to 7 T in steps of 0.1 T up to 4 T followed by steps of 0.2 T up to 5 T, as well as 5.25, 5.5, 6, 6.5, and 7 T. The transients are well fitted by a single exponential decay according to

$$I(t) = A_0 \exp\left(-\frac{t}{\tau}\right) + y_0. \tag{5}$$

The decay times of the WW range from 75 ps for the dqw10 to 110 ps for the dqw5 in zero field whereas at 7 T they all have almost the same time constants of about 95 ps (see also Fig. 9). For $B < B_x$ the time constants for the WW excitons increase slightly because the the recombination probabilities are reduced as afore discussed. The time constants decrease due to higher transition probability between el_ and hh_ for applied fields $B > B_x$ beyond the lh-hh crossover. The transition from type I to type II leads to a very strong increase in the time constants for the sample dqw10. It has more influence on the time constants than the transition from lh to hh exciton. The NW signals of all samples show an increase in the time constants with increasing magnetic field due to the less energy channel to the Mn subsystem. The decay times of the NW are displayed in Fig. 10. The sample dqw5 has a time constant of 4.2 ps by 0 T up to 8.5 ps at 7 T. For the samples dqw10 and dqw100 the times range between 9.0 to 16.6 ps and 12.4 to 22.6 ps, and between 0 and 7 T, respectively. Also, the decay time of the barrier signal increases with increasing magnetic field (not shown here). The time-resolved measurements thus corroborate all the results of the CW measurements.

In conclusion, the energy transfer processes in ZnSe/(Zn,Mn)Se DQW heterostructures under the influence of external magnetic fields are investigated. The PL is governed by the interplay of the lh-hh crossover in the WWs, the energy transfer to the Mn subsystem, and the type I-type II transition. The tunneling process itself plays only a minor role and is camouflaged by the other effects. The steady-state results are corroborated by TR PL measurements and QW calculations.

[1] S. Ten, F. Henneberger, M. Rabe, and N. Peyghambarian, Phys. Rev. B **53**, 12637 (1996).
[2] T. M. Kim, S. H. Lee, and H. L. Park, Solid State Commun. **101**, 531 (1997).
[3] W. Heimbrodt, O. Goede, T. Köpp, K. Hieke, B. Lunn, and T. Gregory, J. Cryst. Growth **117**, 859 (1992).
[4] W. Heimbrodt, L. Gridneva, M. Happ, N. Hoffmann, M. Rabe, and F. Henneberger, Phys. Rev. B **58**, 1162 (1998).
[5] D. Suisky, W. Heimbrodt, C. Santos, F. Neugebauer, M. Happ, B. Lunn, J. E. Nicholls, and D. E. Ashenford, Phys. Rev. B **58**,

3969 (1998).
[6] G. Aliev, J. Puls, L. Parthier, F. Henneberger, and W. Heimbrodt, Physica E (Amsterdam) **10**, 511 (2001).
[7] Ł. Kłopotowski, J. Suffczyński, M. Nawrocki, and E. Janik, J. Supercond. **16**, 435 (2003).
[8] M. Nawrocki, Ł. Kłopotowski, and J. Suffczyński, Phys. Status Solidi B **241**, 680 (2004).
[9] W. M. Chen, I. A. Buyanova, K. Kayanuma, K. Nishibayashi, K. Seo, A. Murayama, Y. Oka, A. A. Toropov, A. V. Lebedev, S. V. Sorokin, and S. V. Ivanov, Phys. Rev. B **72**, 073206 (2005).
[10] A. Saffarzadeh, M. Bahar, and M. Banihasan, Physica E (Amsterdam) **27**, 462 (2005).
[11] I. I. Reshina, S. V. Ivanov, D. N. Mirlin, I. V. Sedova, and S. V. Sorokin, Phys. Rev. B **74**, 235324 (2006).
[12] I. Lawrence, S. Haacke, H. Mariette, W. W. Rühle, H. Ulmer-Tuffigo, J. Cibert, and G. Feuillet, Phys. Rev. Lett. **73**, 2131 (1994).
[13] I. Lawrence, G. Feuillet, H. Tuffigo, C. Bodin, J. Cibert, P. Peyla, and A. Wasiela, Superlattices Microstruct. **12**, 119 (1992).
[14] S. V. Railson, D. Wolverson, J. J. Davies, D. Ashenford, and B. Lunn, Superlattices Microstruct. **13**, 487 (1993).
[15] S. Weston, J. Nicholls, M. O'Neill, T. Stirner, P. Harrison, W. Hagston, J. Hogg, B. Lunn, D. Ashenford, and K. Hieke, J. Phys. IV **3**, 401 (1993).
[16] I. Lawrence, W. W. Rühle, G. Feuillet, H. Tuffigo, H. Mariette, C. Bondin, and J. Cibert, J. Phys. IV **3**, 405 (1993).
[17] K. Hieke, W. Heimbrodt, I. Lawrence, W. W. Rühle, T. Pier, H.-E. Gumlich, D. E. Ashenford, and B. Lunn, Solid State Commun. **93**, 257 (1995).
[18] K. Hieke, W. Heimbrodt, T. Pier, H.-E. Gumlich, W. W. Rühle, J. E. Nicholls, and B. Lunn, J. Cryst. Growth **159**, 1014 (1996).
[19] Th. Förster, Z. Naturforsch. **4a**, 321 (1949).
[20] D. L. Huber, Phys. Rev. B **20**, 2307 (1979).
[21] P. J. Klar, D. Wolverson, J. J. Davies, W. Heimbrodt, and M. Happ, Phys. Rev. B **57**, 7103 (1998).
[22] J. K. Furdyna, J. Appl. Phys. **64**, R29 (1988).
[23] O. Goede and W. Heimbrodt, Phys. Status Solidi B **146**, 11 (1988).
[24] J. Gaj, R. Planel, and G. Fishman, Solid State Commun. **29**, 435 (1979).
[25] V. V. Rossin, T. Bottger, and F. Henneberger, Phys. Rev. B **54**, 7682 (1996).
[26] W. Heimbrodt, O. Goede, V. Weinhold, K. Hieke, M. Happ, N. Hoffmann, J. Griesche, and K. Jacobs, J. Lumin. **60-61**, 344 (1994).
[27] P. J. Klar, D. Wolverson, J. J. Davies, W. Heimbrodt, M. Happ, and T. Henning, Phys. Rev. B **57**, 7114 (1998).
[28] E. Deleporte, T. Lebihen, B. Ohnesorge, Ph. Roussignol, C. Delalande, S. Guha, and H. Munekata, Phys. Rev. B **50**, 4514 (1994).
[29] V. V. Rossin, F. Henneberger, and J. Puls, Phys. Rev. B **53**, 16444 (1996).
[30] H. Falk, J. Hübner, P. J. Klar, and W. Heimbrodt, Phys. Rev. B **68**, 165203 (2003).